RSC Advances

PAPER

View Article Online
View Journal | View Issue

Cite this: *RSC Adv.*, 2017, **7**, 21446

A highly zinc-selective ratiometric fluorescent probe based on AIE luminogen functionalized coordination polymer nanoparticles†

Na Lin, Qin Zhang, Xin Xia, Mengyu Liang, Shihong Zhang, Liyan Zheng, * Qiue Cao* and Zhongtao Ding

Received 22nd December 2016
Accepted 9th April 2017

DOI: 10.1039/c6ra28551a

rsc.li/rsc-advances

Coordination polymer nanoparticles (CPNs) formed by self-assembly of metal ions (or clusters) and organic bridging ligands through coordination bonds provide a unique platform for designing multifunctional nanoparticles. In this work, we report a ratiometric fluorescent probe for Zn^{2+} based on CPNs, which were prepared from AIE fluorophore HDBB molecules with metal ions. The CPNs are composed of HDBB molecules with Tb^{3+} (named Tb-HDBB-CPNs) which displayed a matrix coordination-induced emission peak at a wavelength of 590 nm, while CPNs formed by HDBB molecules and Zn^{2+} (named Zn-HDBB-CPNs) showed a distinctive fluorescent property with a blue emission peak wavelength of 470 nm. Based on the cation exchange process of Tb-HDBB-CPNs with Zn^{2+}, a highly selective ratiometric fluorescent probe for the determination of Zn^{2+} in aqueous solution was developed with a linear range from 0.1 to 60 μM and a detection limit of 50 nM. Our approach using AIE molecules as organic ligands for the construction of CPNs paves a way toward AIE functionalized materials with ratiometric fluorescence response and will find wide applications in chemical sensing.

1. Introduction

Coordination polymer nanoparticles, which are made from metal ions (or clusters) connected by organic ligands, have attracted growing interest because of their structural tailorability with different morphologies and physicochemical properties.[1,2] To date, CPNs have been widely studied for their potential applications in gas storage and separation, heterogeneous catalysis, chemical sensing, biomedical imaging and drug delivery.[3–11] Nevertheless, the rational design of functional coordination polymers nanoparticles is still in an premature, primary stage.[12] Fluorescent CPNs have demonstrated their considerable potential in chemical sensing because of their hybrid structures that can offer tunable fluorescence and have been investigated in the determination of ion, drug and enzyme activity.[13–16] However, the development of fluorescent CPNs has suffered from the problem of aggregation-caused quenching (ACQ), in which chromophores that show high fluorescence quantum yields in dilute solutions become nonfluorescent in the colloidal or solid state, where intermolecular interactions, such as π-stacking, often cause self-quenching.[17,18]

The concept of aggregation-induced emission or aggregation-induced enhanced emission (AIEE) has emerged to be a powerful and versatile strategy for the design of novel types fluorescent probes and luminescent materials to overcome ACQ problem.[19–21] In this process, the fluorogens are almost non-emissive as individual molecule because of the nonradiative decay through intramolecular motion. Such intramolecular motion can be restricted once these molecules aggregate together, resulting in strong fluorescence. A typical example is tetraphenylethene (TPE) molecule, a well-known AIE fluorogen, in which the olefin stator is surrounded by phenyl rotors and the restriction of intramolecular motion (RIM) is known to account for its strong fluorescence in colloids and in the solid state.[22,23] AIE-based luminescent materials not only avoid the ACQ problem caused by aggregation but also provide new approaches based on turn-on mode in the applications of chemical sensors,[24–29] biological probes,[30–33] and solid-state emitters.[34,35]

Recently, some TPE-based AIE molecules were utilized as organic ligands in the construction of metal–organic frameworks (MOFs), which is an intriguing class of inorganic–organic hybrid crystalline materials.[36,37] These studies demonstrated that rigidifying AIE molecules as fluorescent links by MOFs formation efficiently and substantially tune the electronic transition energies and raise the florescent quantum yield, owing to twisted linker conformation, intramolecular hindrance, and framework rigidity.[38] The applications of TPE-based MOFs with excellent luminescent behaviors are well explored as light-emitting diodes (LED), drug vehicles and

Key Laboratory of Medicinal Chemistry for Natural Resource (Yunnan Univeristy), Ministry of Education, School of Chemical Science and Technology, Yunnan University, Kunming, Yunnan 650091, P. R. China. E-mail: zhengliyan@ynu.edu.cn; qecao@ynu.edu.cn

† Electronic supplementary information (ESI) available. See DOI: 10.1039/c6ra28551a

chemical sensor.[39–42] On the other hand, to the best of our knowledge, the utilization of AIE molecules as organic ligands in the amorphous CPNs has not been investigated. Different from the crystal CPNs with static structures, the amorphous CPNs exhibit a higher level of structural tailorability. Their structures can be depolymerized much faster under milder conditions.[43] Moreover, the preferred turn-on responsive fluorescence when exposed to analytes was not obvious due to the almost complete restriction of intramolecular motion (RIM) in the ligands after MOFs formation.[39,40] One way to overcome this disadvantage is developing ratiometric fluorescent probes, which display two distinctly different measurable signals in the presence and absence of analyte.

Zinc is the second most abundant heavy metal ion, after iron, in the human body and plays important roles in various biological systems. It is an essential element required by all cells with various functions, for example, the control of gene transcription, metalloenzyme function and synaptic vesicles in excitatory nerve terminals.[44] Thus, zinc ions are important analyte from the view of biochemistry, medicine and environment.[45] Taking envisaged applications into account, especially interesting are zinc ions probes operating in ratiometric fluorimetric mode.[46]

Herein, we report a new type AIE-based CPNs that is prepared from AIE fluorophore HDBB molecules with metal ions. Tb-HDBB-CPNs and Zn-HDBB-CPNs emit different wavelength fluorescence in aqueous solution upon excitation with 365 nm light. The cation exchange process of these AIE-based CPNs were studied by fluorescence emission spectra, energy-dispersive X-ray (EDX) spectra, and inductively coupled plasma (ICP) measurement. A ratiometric fluorescent probe for the detection of Zn^{2+} was developed on the basis of cation exchange process of Tb-HDBB-CPNs with Zn^{2+}.

2. Experimental section

2.1 Chemicals and materials

2,4-Dihydroxybenzaldehyde, 4-carboxybenzaldehyde, terbium nitrate pentahydrate, zinc nitrate pentahydrate, disodium hydrogen phosphate and sodium dihydrogen phosphate were purchased from Aladdin. 4-Formyl-3-hydroxybenzoic acid were purchased from Bide pharmatech. All other reagents were of analytical grade and used as received. Doubly distilled water was used throughout the experiments. Tris–HCl (Tris = 2-amino-2-hydroxymethylpropane-1,3-diol) buffered solutions were prepared by titrating 0.01 M Tris solutions with a concentrated HCl (1 M) to the required pH values.

2.2 Apparatus

X-ray powder diffraction patterns were taken using a D/max-TTR III X-ray diffractometer (Rigaku, Japan) with a scan speed of 0.1 s per step and a step size of 0.01°. The morphology and composition element of CPNs were characterized by field emission scanning electron microscopy (SEM) (JEM-2100F). The Fourier transform infrared (FT-IR) spectra were obtained on a FT-IR spectrophotometer (Thermo Nicolet 365). UV-Vis absorption was characterized using a UV/Vis/NIR spectrophotometer (Shimadzu, Japan). Fluorescence spectra were recorded on a Hitachi High-Technologies Corporation Tokyo Japan 5J2-0004 model F-7000 FL spectrofluorometer. Fluorescence emission lifetimes were determined on an Edinburgh Analytical Instrument (FLS900 fluorescence spectrometer) with a light-emitting diode lamp (405 nm) and analyzed by the use of a program for exponential fits. ICP-1000 system (Shimadzu, Japan) was utilized to the detection of metal ion concentration. Particle size distribution of HDBB-CPNs was recorded by a dynamic light scattering instrument (BI-90 Plus, Brookhaven Instruments Corp).

2.3 Synthesis of HDBB, L2 and L3

The synthesis of HDBB (4,4′-(hydrazine-1,2-diylidene bis (methanylylidene)) bis (3-hydroxybenzoic acid)), L2 and L3 were the same as our previous report.[47] Typically, 4-formyl-3-hydroxybenzoic acid (166.2 mg, 1.0 mmol) was dissolved in methanol (10 mL). Then hydrazine hydrate (24 μL, 0.5 mmol; 80%) was added and refluxed at 75 °C. After refluxing overnight, the resulting precipitate was filtered and washed with 30 mL methanol. After drying, HDBB was obtained as a yellow powder. The molecular structures of HDBB, L2 and L3 was verified by NMR and mass spectroscopy.

2.4 Preparation of CPNs

The preparation of the AIE-based CPNs was performed as reported previously.[15] Briefly, Tb-HDBB-CPNs was synthesized by mixing an aqueous solution of $Tb(NO_3)_3 \cdot 6H_2O$ (26.11 mg, 0.06 mmol) with Tris buffer (10 mL) containing HDBB (3.28 mg, 0.01 mmol), adjusting the pH value to 9.0 to keeping HDBB molecules at dissolved state, and then stirring 2 hours at room temperature to form a yellow suspension. The resulting precipitate was then centrifuged and washed with pH 9.0 Tris buffer solution several times. For the preparation of Zn-HDBB-CPNs, the $Tb(NO_3)_3 \cdot 6H_2O$ was replaced by $Zn(NO_3)_3 \cdot 6H_2O$ (11.36 mg, 0.06 mmol) and also get a yellow suspension. The dynamic light scattering measurement has been applied to investigate the stability of these CPNs. The particle sizes of Tb-HDBB-CPNs were about 50 ± 5 nm and 663 ± 28 nm after storing one month and three months in doubly distilled water at 4 °C (Fig. S1†). Zn-HDBB-CPNs displayed similar tendency. These results indicated that the HDBB-CPNs remained stable at least one month.

2.5 Quantification of HDBB, Tb^{3+}, and Zn^{2+} in CPNs

HDBB molecules were dissolved in pH 11.0 0.1 M phosphate buffer solution to obtain a series of HDBB solutions with concentrations ranging from 5.0 to 200.0 μM. Absorption spectra were recorded with a UV-Vis spectrophotometer. The standard curves were plotted from linear fitting of the absorbance at 365 nm as a function of HDBB concentrations. The samples of Tb-HDBB-CPNs and Zn-HDBB-CPNs were dissolved in pH 11.0 0.1 M phosphate solution. The amounts of HDBB, Tb^{3+} and Zn^{2+} in these samples was quantified using UV-Vis spectrophotometer and ICP measurement, respectively.

2.6 Fluorescence quantum yield

The fluorescence quantum yield was calculated from the relation:

$$\phi_x = \phi_s \left(\frac{n_x}{n_s}\right)^2 \left(\frac{A_s}{A_x}\right) \left(\frac{F_x}{F_s}\right)$$

where the subscripts s and x indicate the standard and text respectively, ϕ is the fluorescence quantum yield, A corresponds to the absorbance of the solution, F is the fluorescence intensity, and n is the refractive index of the solvent. The quantum yields of Tb-HDBB-CPNs and Zn-HDBB-CPNs are 14.27% and 17.25%, respectively.

2.7 Analysis of real sample

A water sample was collected from Green Lake (Yunnan, China). The sample was filtered through a 0.22 μm membrane (Millipore) prior to be detected. One hundred microliters of the above water sample was added to 900 μL of Tris buffer solution (10 mM, pH = 7.0) containing Tb-HDBB-CPNs (20 μg mL^{-1}) and then analyzed using the developed detection method.

3. Results and discussion

3.1 Preparation and characterization of AIE-based CPNs

A typical route for preparing CPNs is shown as Scheme 1. The Tb-HDBB-CPNs were prepared from HDBB (L1) and terbium nitrate hexahydrate in pH 9.0 Tris buffer solution at room temperature by self-assembly process. The resulting yellow products were purified by centrifugation and washed several times with Tris buffer solution (pH = 9.0). The resulting CPNs were suspended in aqueous solution and could be stored at 4 °C for three months without any changes. The control experiment showed that no CPNs were obtained in the absence of HDBB molecules or Tb^{3+}, suggesting that both HDBB and Tb^{3+} are essential for the construction of CPNs. The FT-IR spectrum (Fig. 1A and B) measurement of the as-prepared Tb-HDBB-CPNs confirm the coordination of the carboxylate groups to Tb^{3+}, as evidenced by a shift in the C–O stretching frequency to 1650 cm^{-1}. Note that the original C–O stretching frequency of the uncoordinated HDBB was observed at 1692 cm^{-1}. The peak located at 1435 cm^{-1} also indicated the presence of deprotonated carboxylic acid bonded within the CPNs.[48] Zn-HDBB-CPNs show similar IR absorbance behaviors with the one of Tb-HDBB-CPNs,

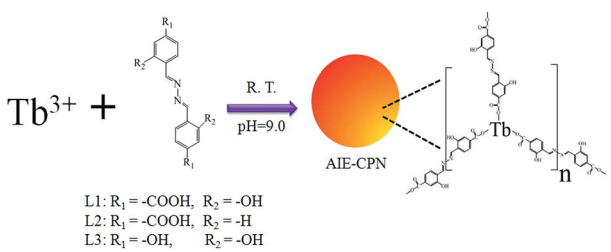

Scheme 1 Schematic representation of the preparation of AIE-based CPN.

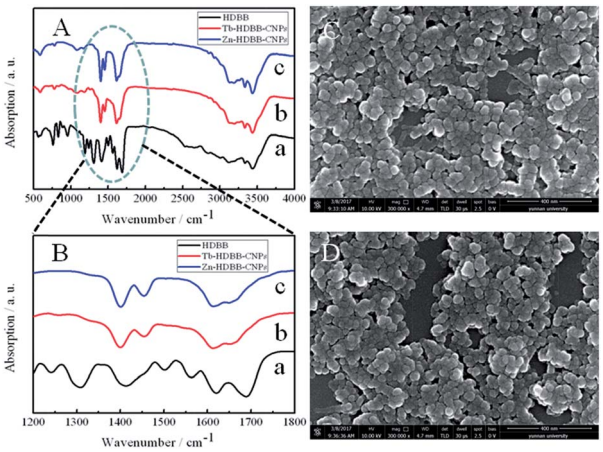

Fig. 1 (A) and (B) FTIR spectra of HDBB (a), Tb-HDBB-CPNs (b), and Zn-HDBB-CPNs (c). FE-SEM images of Tb-HDBB-CPNs (C) and Zn-HDBB-CPNs (D).

suggesting that the formation of Zn-HDBB-CPNs was underwent similar coordination process between HDBB molecule with Zn^{2+}. To further validate the effect of carboxylate group on the formation of these CPNs, two salicylaldehyde hydrazine derivatives (L2, L3) were designed as organic links in the preparation of CPNs (Scheme 1). The experiment results demonstrate that CPNs can be formed in the presence of L2 with Tb^{3+}, however, there were no CPNs obtained under similar condition with the replacement of L1 by L3 due to the lack of carboxylate group in *para*-position of L3. From these results, we can conclude that carboxylate group is essential for the formation of these CPNs.

The SEM images of Tb-HDBB-CPNs and Zn-HDBB-CPNs show typically spherical morphology with relatively uniform size of 50 nm and 55 nm, respectively (Fig. 1C and D). The chemical composition of these CPNs was determined by energy-dispersive X-ray (EDX) analysis during SEM measurement (Fig. S2 and S3†), which demonstrates the presence of Tb and Zn element, further indicating that Tb and Zn ions were involved in the construction of Tb-HDBB-CPNs and Zn-HDBB-CPNs, respectively. The lack of diffraction peaks in powder X-ray diffraction (PXRD) measurement of these CPNs reveals the amorphous structure of these nanoparticles (Fig. S4†).

To further elucidate the structure of these CPNs, the amounts of HDBB molecules and metal ions in these CPNs were quantified using UV-Vis spectra and ICP measurement (Fig. S5–S7†), respectively. The ratios of metal ions to HDBB molecules in these CPNs are about 1 : 1.5 for Tb-HDBB-CPNs and 1 : 1 for Zn-HDBB-CPNs. As a result, the HDBB molecules were in the negative state in the preparation condition (pH = 9.0) of these AIE-based CPNs, and the cations electrostatically attached to the HDBB molecule forming these CPNs. Therefore, the formation of these AIE-based coordination polymers mediated by strong metal–ligand bonding is dominant in the self-assembly process. According to the above results, the structure of Tb-HDBB-CPNs can be proposed and shown in Scheme 1.

3.2 Photochemical properties of AIE-based CPNs

To investigate photochemical properties of these AIE-based CPNs, the fluorescence and absorption spectra were measured. The absorption spectra of these AIE-based CPNs exhibit two peaks at 310 nm and 365 nm (Fig. 2B), which are the same to that of HDBB,[47] and the absorption intensities are slightly increasing. These absorptions can be ascribed to the p–p* and n–p* transitions of the entire molecule.

The fluorescence spectra shows that the maxima emission and excitation of Tb-HDBB-CPNs are at 590 nm and 365 nm (Fig. 2A), which are similar to the precursor HDBB. The fluorescence quantum yield of Tb-HDBB-CPNs is 14.27% in aqueous solution, which is about three times larger than the one of HDBB (5.32%). The fluorescence enhancement of Tb-HDBB-CPNs can be attributed to the immobilization of the HDBB linker as it is strongly coordinated to Tb^{3+}. The formation of rigid CPNs *via* coordination of HDBB to Tb^{3+} prevents the torsional relaxation, thus the RIM process is activated. The fluorescence lifetime of Tb-HDBB-CPNs (2.92 ns) is longer than the one of HDBB molecules (1.97 ns) (Fig. S8†). After coordinating with Tb^{3+}, the radiative rate constant (k_r) of the HDBB increased from 27.0×10^6 s^{-1} to 48.86×10^6 s^{-1}, but the non-radiative rate constant (k_{nr}) decreased from 4.80×10^8 s^{-1} to 2.94×10^8 s^{-1} (Table S1†).

These results are similar with previous reports, the lifetime and fluorescence quantum yield of many AIE molecules usually increase after aggregation owing to the reducing non-radiative processes and activating the radiative channel.[19] Consequently, the formation of CPNs prevents the HDBB excited state distortion, hence the exciton immediately released the energy *via* fluorescence and results in a higher fluorescence quantum yield and longer lifetime.

Unlike Tb-HDBB-CPNs emit yellow fluorescence measured at 590 nm, the Zn-HDBB-CPNs emit blue lights observed at 470 nm, which is almost 120 nm blue-shifted (Fig. 2A). The maximum excitation wavelength of Zn-HDBB-CPNs is retained at 365 nm, which is consistent with its absorption spectrum. The lifetime and fluorescence quantum yield are 17.25% and 1.01 ns (Fig. S9†). The radiative rate constant and non-radiative rate constant of Zn-HDBB-CPNs were 172.5×10^6 s^{-1} and 8.19 $\times$ 10 s^{-1}, respectively. This distinct emission can be ascribed to the inhibition of photo-induced electron transfer process after HDBB coordinating with Zn(II); two nitrogens on hydrazone moiety in HDBB molecule as well as phenolic oxygen may participate in binding to Zn^{2+}.[49,50]

3.3 Sensing mechanism of ratiometric fluorescent probe for Zn^{2+}

Cation exchange in CPNs and MOFs has become a powerful method tuning their composition, functionality and porosity.[6,51,52] We hypothesized that cation exchange process also can occur in our AIE-based CPNs. In a typical reaction, we prepared a mixture of Tb-HDBB-CPNs and 0.15 mM Zn^{2+} in pH 7.0 Tris buffer solution under ambient conditions. After 3 h of cation exchange, the resulted CPNs were separated from the mixture by centrifugation. Fluorescence emission spectra, SEM, EDX spectra and ICP spectra were measured before and after cation exchange reaction of the CPNs sample. As shown in Fig. 3A, fluorescence emission centered at 470 nm increased remarkably with a decrease of fluorescence emission at 590 nm under the excitation wavelength at 365 nm. The dual emission spectrum of the resulting particles reveals successful cation exchange of Tb-HDBB-CPNs by Zn^{2+}, consequently, blocking of photo-induced electron transfer process of HDBB molecules. Furthermore, the morphology of Tb-HDBB-CPNs after Zn^{2+} exchange is not much different from the one of before exchange (Fig. S10†). A relating EDX spectrum of the Tb-HDBB-CPNs measured after the cation exchange shows the expected Zn signal, meanwhile, Tb signal is also can be observed in the EDX spectrum (Fig. S11†). Finally, Tb signal observed in ICP spectrum of Tb-HDBB-CPNs supernatant after cation exchange is much larger than the one of control experiment without adding Zn^{2+}, indicating that partly cation exchange of Tb-HDBB-CPNs by Zn^{2+}. These experiments provided direct evidences of cation exchange in Tb-HDBB-CPNs with Zn^{2+}. Thus, the cation exchange process of Tb-HDBB-CPNs is demonstrated as in Fig. 3B. Briefly, upon the addition of Zn^{2+}, some carboxylic group on the surface of Tb-HDBB-CPNs bind to Zn^{2+} resulting in the formation Zn-Tb-HDBB-CPNs with dual emission fluorescent behavior. As a result, our strategy not only provides a facile route to introduce desired functionality into CPNs but also promotes the potential of CPNs for application, such as ratiometric fluorescence detection.

3.4 Optimization for Zn^{2+} ion detection

As is demonstrated above, the successful cation exchange process of Tb-HDBB-CPNs by Zn^{2+}, inducing the increasing

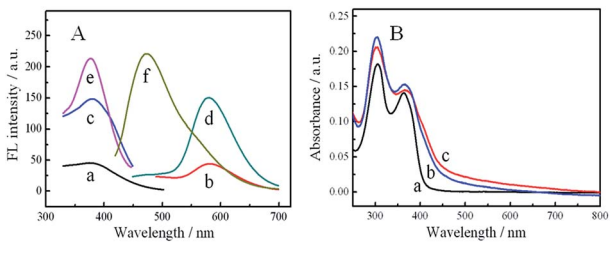

Fig. 2 (A) Excitation and emission spectra of 0.1 mM HDBB (a and b), 0.035 mg mL^{-1} Tb-HDBB-CPNs (c and d), and 0.035 mg mL^{-1} Zn-HDBB-CPNs (e and f). The emission spectra were recorded at 365 nm excitation wavelength. (B) UV-Vis spectra of 0.1 mM HDBB (a), 0.035 mg mL^{-1} Tb-HDBB-CPNs (b), and 0.035 mg mL^{-1} Zn-HDBB-CPNs (c).

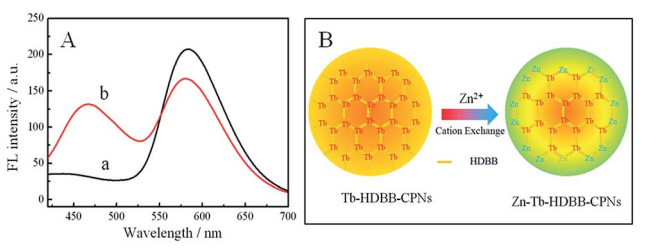

Fig. 3 (A) Fluorescence emission spectra of 0.035 mg mL^{-1} Tb-HDBB-CPNs in the absence (curve a) and presence of 0.15 mM Zn^{2+} (curve b). (B) Schematic representation of the cation exchange process of Tb-HDBB-CPNs with Zn^{2+}.

fluorescence at 470 nm and the decreasing emission at 590 nm, prompted us to apply this AIE-based CPNs for the detection of Zn^{2+} in aqueous solution. We can image that the ratios of I_{470} to I_{590} (*i.e.*, I_{470}/I_{590}) would be closely associated with the degree of the exchange of the Tb-HDBB-CPNs caused by Zn^{2+}, as a consequence, which could be used for the ratiometric fluorescence assay of Zn^{2+}.

Fig. 4A depicts the typical time-dependent fluorescent intensity at 470 nm of the Tris buffer containing Tb-HDBB-CPNs after the addition of Zn^{2+} into the buffer. Upon the addition of Zn^{2+} the fluorescent spectrum of the Tb-HDBB-CPNs was recorded immediately and every on minute consecutively at room temperature. After adding Zn^{2+}, the fluorescent intensity at 470 nm of Tb-HDBB-CPNs was enhanced significantly and reached a plateau after 2 min. The fast fluorescence response can be ascribed to the unique amorphous structure of Tb-HDBB-CPNs.

We next examined the effects of other metal ions on the fluorescence intensity of Tb-HDBB-CPNs under identical conditions. As shown in Fig. 4B, only the addition of Zn^{2+} resulted in a significant fluorescence enhancement at 470 nm; no remarkable changes in the fluorescence of Tb-HDBB-CPNs were observed upon the addition of other metal ions, including Co^{2+}, Mg^{2+}, K^{+}, Fe^{3+}, Ni^{2+}, Ca^{2+}, Cd^{2+}, Pb^{2+}, Hg^{2+}, and Cu^{2+}. The high selectivity of Tb-HDBB-CPNs to Zn^{2+} is attributed to the special fluorescent behavior of the coordination compound of Zn^{2+} with HDBB.

The fluorescence response of Tb-HDBB-CPNs to Zn^{2+} in different concentrations is shown as Fig. 4C. Corresponding to the decreased fluorescence at 590 nm, the fluorescence at 470 nm was enhanced gradually with the increase of Zn^{2+} concentrations from 0 to 60 μM. There is a linear ratio fluorescence response to Zn^{2+} in the concentration range 0.1–60 μM. The detection limit is 50 nM on the basis of a signal-to-noise ratio of 3 : 1. This detection limit satisfies the maximum permitted level of 5 mg L^{-1} Zn^{2+} in drinking water regulated by the U.S. Environmental Protection Agency (EPA).[45]

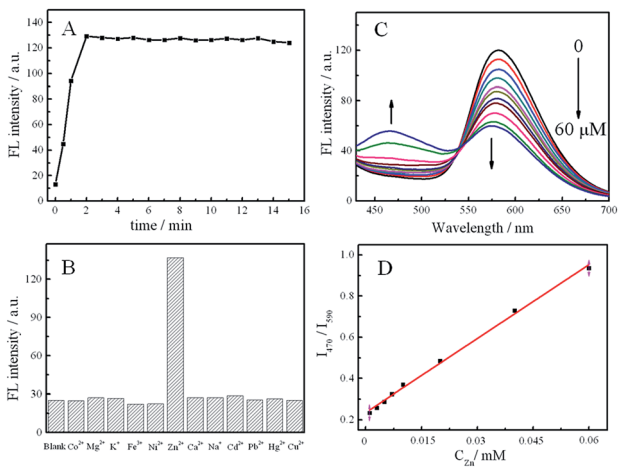

Fig. 4 (A) Time-dependent fluorescence at 470 nm response of the 0.02 mg mL^{-1} Tb-HDBB-CPNs to 0.1 mM Zn^{2+} in pH 7.0 Tri buffer solution. (B) The selectivity of Tb-HDBB-CPNs based sensor for Zn^{2+} to other cations in pH 7.0 Tri buffer solution. The concentrations of Tb-HDBB-CPNs, Zn^{2+} and other cations were 0.02 mg mL^{-1}, 0.15 mM and 0.25 mM, respectively. (C) Fluorescence emission spectra of Tb-HDBB-CPNs probe exposed to various concentrations of Zn^{2+}. These spectra were measured in pH 7.0 Tri buffer solution. The concentration of Tb-HDBB-CPNs was 0.02 mg mL^{-1}. The concentration of Zn^{2+} were 0, 0.1, 0.5, 1.0, 3.0, 5.0, 7.0, 10, 20, 40, 60 μM. (D) The linear plot of the value of I_{470}/I_{590} *versus* the concentration of Zn^{2+}.

3.5 Application in water samples

It is very important to monitor the level of Zn^{2+} in water samples, because Zn^{2+} in human bodies tend to bio-accumulate and damage central nervous system, blood composition, lungs, kidneys and liver. The practicability of Tb-HDBB-CPNs fluorescent nanoprobes was assessed by applying it to the real analysis for Zn^{2+} in water sample of the Green Lake, which is a famous scenic spot of Yunnan Province in China. An average value of 1.48 ± 0.18 μM Zn^{2+} was found for $n = 4$ determinations in the Green Lake water sample using this new approach with good recovery (99.15%), after the subtraction of the interception from that of the standard calibration curve (Fig. 4D), which is consistent with the result obtained by ICP spectroscopic methods, 1.34 ± 0.08 μM. This result suggests that our ratiometric fluorescence nanoprobe can be used for Zn^{2+} determination in water samples.

4. Conclusions

In summary, AIE-based CPNs have been developed by using AIE molecules as bridging ligands. Tb-HDBB-CPNs were further employed as ratiometric fluorescence probe to direct detection of Zn^{2+} in aqueous solution based on cation exchange effect. The ratio fluorescence of Zn-Tb-HDBB-CPNs was enhanced linearly with the Zn^{2+} concentration from 100 nM to 60 μM. The detection limit for Zn^{2+} in aqueous solution is 50 nM. The ratiometric fluorescent probe based on Tb-HDBB-CNPs exhibits the advantages of direct and fast detection procedure, excellent stability and selectivity. The proposed strategy might provide a new platform for the design and application of fluorescent probes based on AIE functionalized coordination polymers.

Acknowledgements

This work was financially supported by the National Natural Science Foundation of China (NSFC, 21405135, 21465025), the Project sponsored by SRF for Yunnan university (2013CK006) and Cultivation Program for Key Young Teachers of Yunnan University (XT412003).

Notes and references

1 M. Oh and C. A. Mirkin, *Nature*, 2005, **438**, 651–654.
2 Y. Liu, F. Boey, L. L. Lao, H. Zhang, X. Liu and Q. Zhang, *Chem.–Asian J.*, 2011, **6**, 1004–1006.
3 I. Imaz, M. Rubio-Martínez, L. García-Fernández, F. García, D. Ruiz-Molina, J. Hernando, V. Puntes and D. Maspoch, *Chem. Commun.*, 2010, **46**, 4737–4739.

4 C. M. Hongliang Tan, Q. Li, L. Wang, F. Xu, S. Chen and A. Song, *Analyst*, 2014, **139**, 5516–5522.
5 K. E. deKrafft, Z. Xie, G. Cao, S. Tran, L. Ma, O. Z. Zhou and W. Lin, *Angew. Chem., Int. Ed.*, 2009, **48**, 9901–9904.
6 M. Oh and C. A. Mirkin, *Angew. Chem.*, 2006, **118**, 5618–5620.
7 N. Lin, J. Li, Z. Lu, L. Bian, L. Zheng, Q. Cao and Z. Ding, *Nanoscale*, 2015, **7**, 4971–4977.
8 L. Xing, Y. Cao and S. Che, *Chem. Commun.*, 2012, **48**, 5995–5997.
9 W. J. Rieter, K. M. Pott, K. M. Taylor and W. Lin, *J. Am. Chem. Soc.*, 2008, **130**, 11584–11585.
10 Y. Liao, L. He, J. Huang, J. Zhang, L. Zhuang, H. Shen and C.-Y. Su, *ACS Appl. Mater. Interfaces*, 2010, **2**, 2333–2338.
11 R. C. Huxford, K. E. Dekrafft, W. S. Boyle, D. Liu and W. Lin, *Chem. Sci.*, 2012, **3**, 198–204.
12 F. Pu, E. Ju, J. Ren and X. Qu, *Adv. Mater.*, 2014, **26**, 1111–1117.
13 H. Tan, B. Liu and Y. Chen, *ACS Nano*, 2012, **6**, 10505–10511.
14 H. Tan, L. Zhang, C. Ma, Y. Song, F. Xu, S. Chen and L. Wang, *ACS Appl. Mater. Interfaces*, 2013, **5**, 11791–11796.
15 J. Deng, P. Yu, Y. Wang and L. Mao, *Anal. Chem.*, 2015, **87**, 3080–3086.
16 R. Nishiyabu, N. Hashimoto, T. Cho, K. Watanabe, T. Yasunaga, A. Endo, K. Kaneko, T. Niidome, M. Murata and C. Adachi, *J. Am. Chem. Soc.*, 2009, **131**, 2151–2158.
17 K. Mizusawa, Y. Takaoka and I. Hamachi, *J. Am. Chem. Soc.*, 2012, **134**, 13386–13395.
18 K. Mizusawa, Y. Ishida, Y. Takaoka, M. Miyagawa, S. Tsukiji and I. Hamachi, *J. Am. Chem. Soc.*, 2010, **132**, 7291–7293.
19 Y. Hong, J. W. Lam and B. Z. Tang, *Chem. Commun.*, 2009, 4332–4353.
20 J. Mei, Y. Hong, J. W. Lam, A. Qin, Y. Tang and B. Z. Tang, *Adv. Mater.*, 2014, **26**, 5429–5479.
21 Z. Luo, X. Yuan, Y. Yu, Q. Zhang, D. T. Leong, J. Y. Lee and J. Xie, *J. Am. Chem. Soc.*, 2012, **134**, 16662–16670.
22 R. Hu, N. L. Leung and B. Z. Tang, *Chem. Soc. Rev.*, 2014, **43**, 4494–4562.
23 N. B. Shustova, T.-C. Ong, A. F. Cozzolino, V. K. Michaelis, R. G. Griffin and M. Dincă, *J. Am. Chem. Soc.*, 2012, **134**, 15061–15070.
24 V. Vij, V. Bhalla and M. Kumar, *ACS Appl. Mater. Interfaces*, 2013, **5**, 5373–5380.
25 Y. Liu, C. Deng, L. Tang, A. Qin, R. Hu, J. Z. Sun and B. Z. Tang, *J. Am. Chem. Soc.*, 2010, **133**, 660–663.
26 Y. Zhang, D. Li, Y. Li and J. Yu, *Chem. Sci.*, 2014, **5**, 2710–2716.
27 L. Zhang, N. He and C. Lu, *Anal. Chem.*, 2015, **87**, 1351–1357.
28 J. Chen, Y. Wang, W. Li, H. Zhou, Y. Li and C. Yu, *Anal. Chem.*, 2014, **86**, 9866–9872.
29 D. G. Khandare, H. Joshi, M. Banerjee, M. S. Majik and A. Chatterjee, *Anal. Chem.*, 2015, **87**, 10871–10877.
30 R. T. Kwok, C. W. Leung, J. W. Lam and B. Z. Tang, *Chem. Soc. Rev.*, 2015, **44**, 4228–4238.
31 J. Liang, B. Z. Tang and B. Liu, *Chem. Soc. Rev.*, 2015, **44**, 2798–2811.
32 D. Ding, K. Li, B. Liu and B. Z. Tang, *Acc. Chem. Res.*, 2013, **46**, 2441–2453.
33 X. Zhang, X. Zhang, S. Wang, M. Liu, Y. Zhang, L. Tao and Y. Wei, *ACS Appl. Mater. Interfaces*, 2013, **5**, 1943–1947.
34 L. Chen, Y. Jiang, H. Nie, R. Hu, H. S. Kwok, F. Huang, A. Qin, Z. Zhao and B. Z. Tang, *ACS Appl. Mater. Interfaces*, 2014, **6**, 17215–17225.
35 D. Li, Y. Zhang, Z. Fan, J. Chen and J. Yu, *Chem. Sci.*, 2015, **6**, 6097–6101.
36 N. B. Shustova, B. D. McCarthy and M. Dinca, *J. Am. Chem. Soc.*, 2011, **133**, 20126–20129.
38 Z. Wei, Z.-Y. Gu, R. K. Arvapally, Y.-P. Chen, R. N. McDougald Jr, J. F. Ivy, A. A. Yakovenko, D. Feng, M. A. Omary and H.-C. Zhou, *J. Am. Chem. Soc.*, 2014, **136**, 8269–8276.
37 Q. Zhang, J. Su, D. Feng, Z. Wei, X. Zou and H.-C. Zhou, *J. Am. Chem. Soc.*, 2015, **137**, 10064–10067.
39 Z. Hu, W. P. Lustig, J. Zhang, C. Zheng, H. Wang, S. J. Teat, Q. Gong, N. D. Rudd and J. Li, *J. Am. Chem. Soc.*, 2015, 16209–16215.
40 X.-G. Liu, H. Wang, B. Chen, Y. Zou, Z.-G. Gu, Z. Zhao and L. Shen, *Chem. Commun.*, 2015, **51**, 1677–1680.
41 L. Wang, W. Wang and Z. Xie, *J. Mater. Chem. B*, 2016, **4**, 4263–4266.
42 N. B. Shustova, A. F. Cozzolino, S. Reineke, M. Baldo and M. Dincă, *J. Am. Chem. Soc.*, 2013, **135**, 13326–13329.
43 A. M. Spokoyny, D. Kim, A. Sumrein and C. A. Mirkin, *Chem. Soc. Rev.*, 2009, **38**, 1218–1227.
44 A. Takeda, M. Nakamura, H. Fujii and H. Tamano, *Metallomics*, 2013, **5**, 417–423.
45 P. Xu, S. Huang, Z. Wang and G. Lagos, *Sci. Total Environ.*, 2006, **362**, 50–55.
46 J. Du, M. Hu, J. Fan and X. Peng, *Chem. Soc. Rev.*, 2012, **41**, 4511–4535.
47 N. Lin, X. Chen, S. Yan, H. Wang, Z. Lu, X. Xia, M. Liang, Y.-L. Wu, L. Zheng and Q. Cao, *RSC Adv.*, 2016, **6**, 25416–25419.
48 C. McKinstry, E. J. Cussen, A. J. Fletcher, S. V. Patwardhan and J. Sefcik, *Cryst. Growth Des.*, 2013, **13**, 5481–5486.
49 X. Cao, X. Zeng, L. Mu, Y. Chen, R. Wang, Y. Zhang, J. Zhang and G. Wei, *Sens. Actuators, B*, 2013, **177**, 493–499.
50 D. Xie, Z. Ran, Z. Jin, X. Zhang and D. An, *Dyes Pigm.*, 2013, **2013**(96), 495–499.
51 M. H. Lee, J. S. Kim and J. L. Sessler, *Chem. Soc. Rev.*, 2015, **44**, 4185–4191.
52 Z. Wang and S. M. Cohen, *Chem. Soc. Rev.*, 2009, **38**, 1315–1329.